Monthly Notices
of the
ROYAL ASTRONOMICAL SOCIETY

MNRAS **482,** 194–205 (2019)
Advance Access publication 2018 October 3

doi:10.1093/mnras/sty2662

Mildly suppressed star formation in central regions of MaNGA Seyfert galaxies

Longji Bing [1,2★] Yong Shi,[1,2★] Yanmei Chen,[1,2] Sebastián F. Sánchez,[3] Roberto Maiolino,[4] Rogério Riffel [5,7] Rogemar A. Riffel [6,7] Dominika Wylezalek,[8] Dmitry Bizyaev,[9,10,11] Kaike Pan[9] and Niv Drory[12]

[1]*School of Astronomy and Space Science, Nanjing University, Nanjing 210093, China*
[2]*Key Laboratory of Modern Astronomy and Astrophysics, Nanjing University, Nanjing 210093, China*
[3]*Instituto de Astronomia, Universidad Nacional Autonoma de Mexico, AP 70-264, 04510 Mexico, DF, Mexico*
[4]*Cavendish Laboratory, University of Cambridge, 19 J. J. Thomson Avenue, Cambridge CB3 0HE, UK*
[5]*Instituto de Física, Universidade Federal do Rio Grande do Sul, Campus do Vale, 91501-970 Porto Alegre, Brasil*
[6]*Laboratório Interinstitucional de e-Astronomia, 77 Rua General José Cristino, 20921-400 Rio de Janeiro, Brasil*
[7]*Departamento de Física, CCNE, Universidade Federal de Santa Maria, 97105-900 Santa Maria, RS, Brazil*
[8]*European Southern Observatory, D-85748 Garching, Germany*
[9]*Apache Point Observatory and New Mexico State University, PO Box 59, Sunspot, NM 88349-0059, USA*
[10]*Sternberg Astronomical Institute, Moscow State University, 119991 Moscow, Russia*
[11]*Special Astrophysical Observatory of the Russian AS, 369167 Nizhnij Arkhyz, Russia*
[12]*McDonald Observatory, The University of Texas at Austin, 1 University Station, Austin, TX 78712, USA*

Accepted 2018 September 28. Received 2018 September 28; in original form 2018 August 1

ABSTRACT

Negative feedback from accretion on to supermassive black holes (SMBHs), that is to remove gas and suppress star formation in galaxies, has been widely suggested. However, for Seyfert galaxies which harbour less active, moderately accreting SMBHs in the local Universe, the feedback capability of their black hole activity is elusive. We present spatially resolved H α measurements to trace ongoing star formation in Seyfert galaxies and compare their specific star formation rate with a sample of star-forming galaxies whose global galaxy properties are controlled to be the same as the Seyferts. From the comparison, we find that the star formation rates within central kpc of Seyfert galaxies are mildly suppressed as compared to the matched normal star-forming galaxies. This suggests that the feedback of moderate SMBH accretion could, to some extent, regulate the ongoing star formation in these intermediate to late type galaxies under secular evolution.

Key words: galaxies: active – galaxies: evolution – galaxies: star formation – galaxies: Seyfert.

1 INTRODUCTION

Supermassive black holes (SMBHs) reside at centres of almost all massive galaxies (Kormendy & Ho 2013).The accretion on to SMBHs, which powers phenomena known as active galactic nuclei (AGNs), is suggested to play key roles in driving galaxy evolution by depositing accretion energy into the interstellar medium (ISM) in AGN host galaxies to regulate star formation (King 2003; Springel 2005; Hopkins et al. 2006). The feedback could be in forms of removing gas from the central part of host galaxies by fast multiphase outflows (Cano-Díaz et al. 2012; Maiolino et al. 2012; Cicone et al. 2014; Carniani et al. 2016), or heating the gas within and surrounding the host galaxies by radio jets (Forman et al. 2007; Fabian 2012). Observations have found the former case in luminous quasars associated with major mergers, while evidence for the latter case mainly comes from radio-loud AGNs reside in massive red elliptical galaxies.

Although AGNs with moderate SMBH accretion (Seyfert galaxies) are much more numerous, their capability of feedback is unclear. It is still unknown if the SMBH's feedback in Seyferts is necessary in re-producing the SMBH-bulge relationships because bulges form through the major merging while Seyfert galaxies are mostly blue and disc dominated spirals in secular evolution (Hopkins et al. 2006; Kormendy & Ho 2013; Heckman & Best 2014). This is in contrast to the case for massive red radio galaxies with elliptical morphology and the remnants of major merging (Springel 2005; Cheung et al. 2016), and luminous quasars that are associated

★ E-mail: ljbing@smail.nju.edu.cn (LB); yong@nju.edu.cn (YS)

with ongoing major merging (Springel 2005; Hopkins et al. 2006). Although outflows of ionized gas are seen in Seyfert galaxies, the observed low outflow rates indicate that they could be driven by the nuclear star formation itself (Harrison et al. 2014; Ho et al. 2014; Wild et al. 2014; López-Cobá et al. 2017a). Some recent spatially resolved studies of a handful nearby Seyferts reveal the existence of fast outflows of ionized or dense molecular gas associated with radio jets but their impacts on star formation are unclear (Christensen et al. 2006; Krause, Fendt & Neininger 2007; Wang et al. 2012; García-Burillo et al. 2014; Morganti et al. 2015; Querejeta et al. 2016; López-Cobá et al. 2017b).

Observationally, it is a big challenge to conclude whether AGN's feedback could regulate star formation or not, and how it regulates star formation. On one hand, if strong outflows emerge, they could clear out the star-forming gas to suppress star formation (Alexander & Hickox 2012; García-Burillo et al. 2014; Alatalo et al. 2015; Hopkins et al. 2016; Wylezalek & Zakamska 2016). The heating by jets propagating through the galaxies could prevent gas from cooling and cut-off the gas supply for further star formation (Karouzos et al. 2014; Choi et al. 2015). On the other hand, the outflows and jets interact with the gas in host galaxies and compress it to trigger new star formation (Silk 2013; Zubovas et al. 2013; Zubovas & Bourne 2017). In fact observations show either no or positive relationships between star formation rates and SMBH accretion rates but no negative trends are seen (Shi et al. 2007, 2009; Baum et al. 2010; Xu et al. 2015; Zhang et al. 2016; Mallmann et al. 2018). Whether AGN's feedback plays the role may also depends on the spatial scale that observations could resolve and time-scale that the observed tracers could probe (Harrison et al. 2012; Cresci et al. 2015; Feruglio et al. 2015). For example, radiation from AGNs nearly instantaneously impact the surrounding ISM while the attenuation from ISM probably limits their impact to the nuclear regions (Roos et al. 2015). Outflows or jets travel slowly and may be decelerated after interactions with ambient gas, which delays their effects on star formation at large distances from the nuclei (Harrison 2017; Harrison et al. 2018). Feedback by jets or outflows on ISM also depends on their orientation relative to the dusty torus, making their effects on star formation to be anisotropic. The short duty cycle of AGNs could also make feedback by radiation from AGNs temporally variable in strength. Case studies of individual AGNs find evidence of coexistence of positive and negative feedback on star formation (Zinn et al. 2013), suggesting the complicated nature of AGN feedback.

The availability of spatially resolved spectra as enabled by integral field unit (IFU) observations offers a new opportunity to investigate the possible effects of AGN's feedback on star formation. These data allow measurements of a range of host galaxy properties in details including the star formation rate, stellar mass, stellar population, and metallicity at kpc scales or smaller and relate them to the AGNs activities (Davies et al. 2007; Dumas et al. 2007; Riffel et al. 2011, 2017; Wylezalek et al. 2017; Sánchez et al. 2018). Especially, a large IFU-observed sample of nearby galaxies from on-going SDSS-IV MaNGA (Bundy et al. 2015) offers the opportunity to statistically explore relationships between AGNs and star formation at kpc scales. In this study, we present studies of spatially resolved star formation activities of nearby Seyfert galaxies and comparisons with a control sample of normal star-forming galaxies. Only with the large number of galaxies observed by MaNGA can we construct such a control sample that all physical parameters that may affect star formation are controlled. In Section 2, we describe the basic information of MaNGA data, the selection of AGNs, and control samples and the procedures of measuring the intensity of spatial resolved star formation. The difference in spatially resolved SFRs between MaNGA AGNs and their comparison samples of normal galaxies are shown in Section 3. We discuss the possible implications of our results in the context of galaxy evolution in Section 4. A flat ΛCDM cosmology with $\Omega_\Lambda = 0.692$, $\Omega_M = 0.308$ and $H_0 = 67.8\,\mathrm{km\,s^{-1}\,Mpc^{-1}}$ is assumed throughout this study.

2 DATA AND METHODS

2.1 MaNGA data

We analysed a large sample of 4756 galaxies with spatially resolved IFU observations carried out by the program of Mapping Nearby Galaxies at Apache Point Observatory (MaNGA) (Bundy et al. 2015; Yan et al. 2016b). MaNGA is an ongoing IFU survey to acquire spatially resolved spectra of nearby ∼100 00 galaxies from 2014 to 2020 (Bundy et al. 2015; Drory et al. 2015; Law et al. 2015; Yan et al. 2016b,a; Blanton et al. 2017), with the Sloan Digital Sky Survey (SDSS) 2.5m telescope (Gunn et al. 2006) and the Baryon Oscillation Spectroscopic Survey (BOSS) spectrograph (Smee et al. 2013; Drory et al. 2015). MaNGA galaxies have a flat distribution in the stellar mass above 10^9 $M_\odot$ and are composed of two sub-samples with different radial coverage: a primary sub-sample of about 70 per cent galaxies ($<z> = 0.03$) with a coverage to 1.5 effective radii (R_e) and a secondary sub-sample of about 30 per cent galaxies ($<z> = 0.04$) with a coverage to 2.5 R_e. The spectrum covers a wavelength range from 3 600 to 10 300 Å with a velocity resolution σ of ∼65 $\mathrm{km\,s^{-1}}$. The spatial resolution is about 2.5 arcmin. The S/N at r band is about 4–8 $\mathrm{Å^{-1}}$ at the edge of the radial coverage.

The raw data were reduced, calibrated, and reconstructed to a data cube by the Data Reduction Pipeline (DRP) (Law et al. 2016). The PIPE3D (Sánchez et al. 2016a,b) was applied to the data cube to measure the continuum and associated physical qualities. Both PIPE3D and MaNGA Data Analysis Pipeline(DAP) (Westfall et al. in preparation) provide measurements on emission line fluxes that we used in sample selection and star formation rate calculation. These measurements were available in the internal MaNGA Product Launch currently at version 6 (MPL_6). These IFU spectra will be released in the coming SDSS DR15.

2.2 The selection of AGNs with star-forming discs

For each MaNGA galaxy, we first constructed the spatially resolved BPT diagram (both NII-BPT and SII-BPT) to classify them into star-forming, composite and AGNs (also LINER) according to the dividing lines in the literature (Baldwin, Phillips & Terlevich 1981; Kauffmann et al. 2003; Kewley et al. 2001, 2006). We used all spaxels with S/N of H α, H β, [O III] 5007Å, and [N II] 6584Å (or [S II] 6717/6731Å) larger than 2 measured by MaNGA DAP using the pure emission line spectrum. A galaxy is classified as an AGN as long as the emission from the central spaxel of the MaNGA datacube has [N II]/H α, [S II]/H α and [O III]/H β line ratios that satisfy: (1) Either the composite or the AGN definition in the [N II]/H α BPT diagram. (2) The AGN or LINER definition in the [S II]/H α BPT-diagram. We also required the equivalent width of H α emission($EW_{\mathrm{H}\,\alpha}$) at the central spaxel to be larger than 3Å, which rejects galaxies with weak emission lines powered by evolved stars (Stasińska et al. 2008; Cid Fernandes et al. 2010; Yan & Blanton 2012; Belfiore et al. 2016). Spaxels classified as 'star formation' are further required to have $EW_{\mathrm{H}\,\alpha} > 6$ Å as suggested by previous studies (Sánchez et al. 2014). We then selected AGNs with

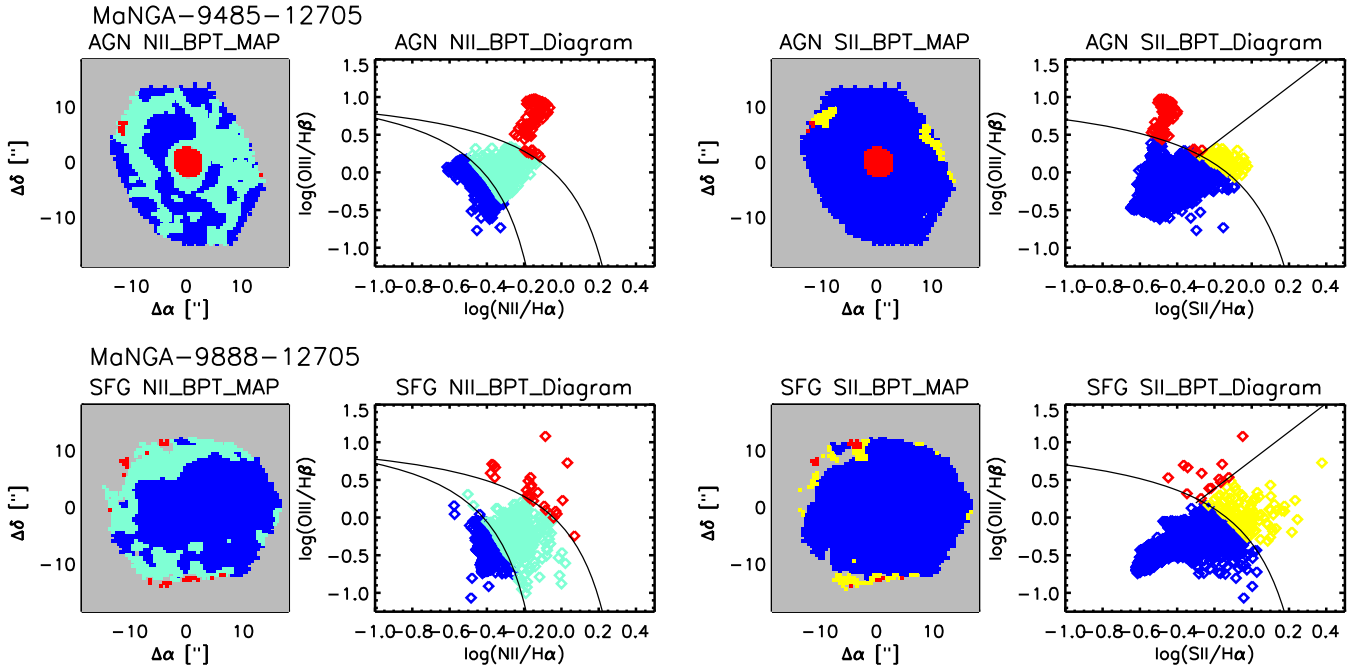

Figure 1. Example BPT maps and diagrams of galaxies selected as our AGN samples and control samples. Ionization in different part of galaxies are classified by BPT diagram, where we mark AGN/Seyfert region in red, LINER region in yellow (only [S II]/H α BPT diagram), composite region in cyan (only [N II]/H α BPT diagram) and star-forming region in blue in resolved BPT map. The lines in BPT diagrams shows the diagnostic criteria from Kauffmann et al. (2003) and Kewley et al. (2006).

star-forming discs as those objects with AGNs present at galaxy centres and star formation in the outer regions to investigate the effects of AGN's feedback on star formation. Quantitatively, we required that more than half of spaxels within 1.0–1.5 R_e should be filled by star formation spaxels, as we need the sSFR at this radial bin to be properly measured to constrain the same parameter in control galaxies to be the same (see Section 2.4 for details). Edge-on galaxies with minor/major axial ratio in NSA catalogue $<$ 0.35 (Blanton et al. 2011) are excluded to eliminate the additional smearing of the light from adjacent radial bins at high inclinations. A total of 56 AGNs are selected under these criteria and an example is shown in Fig. 1.

2.3 The selection bias of the AGN sample

Because the line emission at the centre are contributed not only by the AGN narrow line region but also by star formation, the BPT diagram misses AGNs with high central SFRs. We performed a test to qualify this bias in our sample selection, following the spirit of related methods applied in previous studies (Kauffmann & Heckman 2009; Trump et al. 2015; Davies et al. 2016). We generated simulated AGNs of different [O III] luminosities by adding PSF-convolved point source emission to the emission line maps of pure star-forming galaxies. Given an AGN [O III] luminosity, the point source emission of different emission lines is calculated as following:

(1) For [O III] 5007Å itself, the AGN's contribution is from randomly selected AGN $L_{[O\,III]}$ after the dusty extinction based on the central Balmer decrement (Osterbrock & Ferland 2006) and PSF convolution at g-band available in the MaNGA DRP.

(2) For H β, the AGN's contribution is calculated by the above AGN [O III] 5007Å flux multiplied with a [O III] 5007Å /H β flux ratio. We fixed this ratio to 10 in our simulation, while varying it to other values does not significantly change our result.

(3) For H α, the AGN's contribution is calculated by the above H β flux multiplied with the observed Balmer decrement.

(4) For [N II] 6584Å and [S II] 6717Å +6731Å, the AGN's contribution is measured by the above H α flux multiplied by a representative [N II] 6584Å /H α or ([S II] 6717Å + 6731Å)/H α flux ratio. We fixed these two ratios to the average values of all selected AGNs.

A uniform distribution in the logarithmic [O III] luminosity is applied in the simulation. In total, five luminosity bins were used to cover the range from 7×10^{39} to 7×10^{41} erg s^{-1}. With this simulated AGN sample, we then defined those that satisfied the BPT criteria as the BPT-selected AGNs. Within a [O III] luminosity bin, we measured the central $\Sigma_{H\,\alpha}$ (after attenuation correction) of the BPT-selected AGNs and compared to the central $\Sigma_{H\,\alpha}$ of all AGNs. Fig. 2 shows the distributions of extinction corrected $\Sigma_{H\,\alpha}$ of all simulated AGNs and BPT-selected AGNs. The figure clearly shows lower $\Sigma_{H\,\alpha}$ in BPT-selected AGNs when the AGN [O III] luminosities drop below certain values. It also indicates that the above selection bias becomes less significant in luminous AGNs with the [O III] luminosity above 7×10^{40} ergs s^{-1}. We thus restricted our AGN sample to be above this luminosity in order to avoid the bias towards selecting AGNs with low central SFRs. After applying this luminosity constraint, we got a final AGN sample with 14 objects in total.

2.4 The selection of the comparison sample of pure star-forming galaxies for each AGN

To determine whether the influence on star formation happens in Seyfert galaxies, a well-defined comparison sample of pure

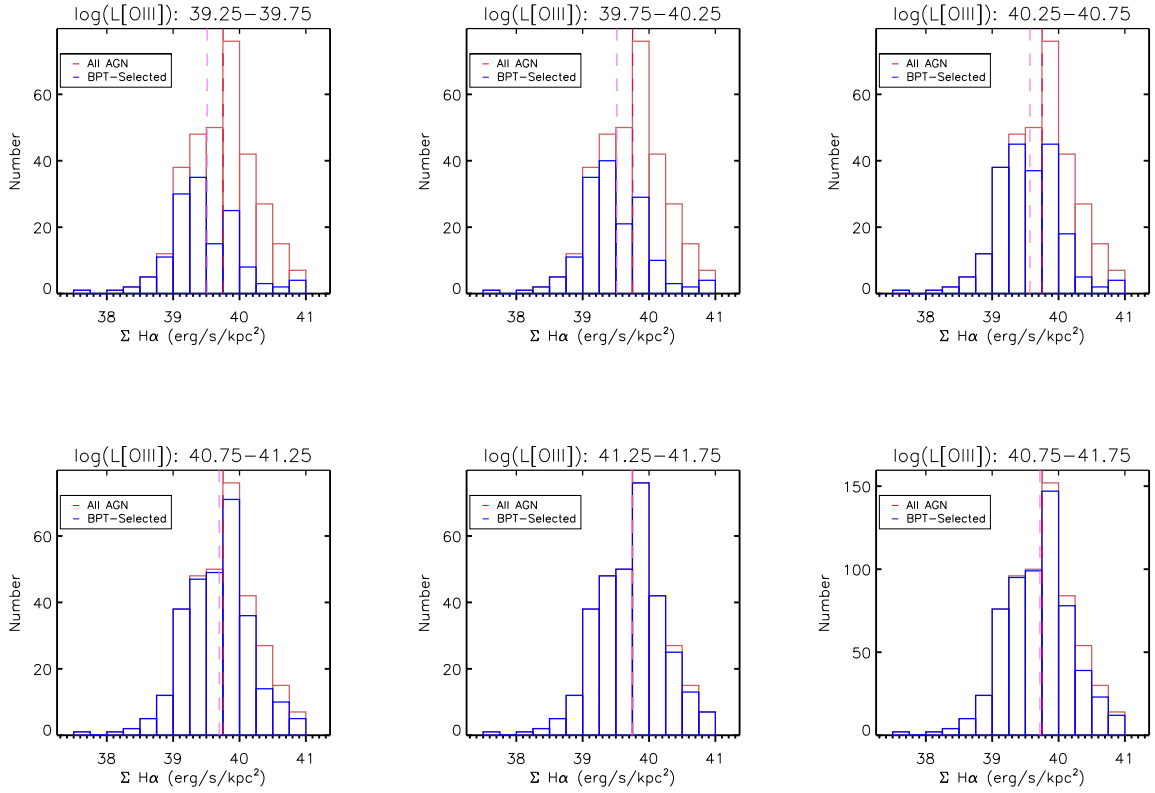

Figure 2. The test on the selection bias of the BPT diagram on central star formation. Blue and red histogram show the distributions of central SFR-related H α surface brightness of all normal galaxies and normal galaxies that are identified as AGNs after adding AGN light. Red and pink vertical lines mark the median value of the distributions. Panels 1–5 show the result of simulation carried out within five luminosity bins. Panel 6 shows the combined result of panels 4 and 5, which supports ignorable bias to lower central star formation rate in BPT selected AGNs at $\log(L_{[\mathrm{O\,III}]} > 40.85)$.

star-forming galaxies without SMBH accretion is needed so that all parameters that affect star formation are controlled to be the same as Seyfert galaxies. We considered six control parameters, including the total stellar mass, the presence/absence of the bar structures, the bulge-to-disc ratio, the stellar mass surface density at $1.5R_e$, the sSFR at $1.5R_e$ and the central stellar mass surface density in defining the control galaxies for each AGN from these pre-selected galaxies with the following quantitative criteria:

(1) The difference of the total stellar mass between each AGN and its comparison galaxies to be within $\Delta\log(M_*)$ <0.3: the galaxy stellar mass controls the overall global galaxy properties to exclude any stellar-mass-dependent effects on the SFRs (Shi et al. 2011, 2018), such as the galaxy metallicity (Shi et al. 2014) and the total SFRs (Brinchmann et al. 2004). The stellar mass measurement was taken from the GALEX–SDSS–WISE legacy catalogue (Salim et al. 2016) based on the UV-optical SED fitting. For galaxies without measurement in Salim et al. (2016), we turned to stellar mass measurement in SDSS + WISE MAGPHYS output catalogue (Chang et al. 2015). Stellar masses from these two studies are consistent with each other over the mass range of MaNGA samples (within 0.2 dex, see section 8 in Salim et al. 2016).

(2) The strength of the bar structures: bars could enhance star formation in the central regions of galaxies (Kennicutt, Tamblyn & Congdon 1994). We required the difference of the debiased vote fraction of 'the existence of bar' from the Galaxy Zoo 2 between each AGN and its comparison galaxies to be lower than 0.25. (Willett et al. 2013).

(3) The difference in bulge-to-disc ratio between each AGN and its comparison galaxies to be within $\Delta B/T < 0.2$. Star formation in bulges is generally lower than in discs. The bulge-to-disc ratio thus relates to the relative level of star-forming activity in the inner parts of galaxies as compared to the outer parts. The bulge-to-disc ratio is based on the *r*-band decomposition of the SDSS images (Simard et al. 2011). For galaxies without B/T measurement in Simard's catalogue, we use the fracDev parameter in *r* band from SDSS DR12 photometric catalogue (Alam et al. 2015) as an alternative control parameter on the bulge-to-disc ratio. Only one of these two parameters is used in the selection of comparison galaxies to a specific sample galaxy.

(4–5) At 1.5 R_e, the difference of the stellar mass surface density between each AGN and its comparison galaxies to be within 0.3 dex ($\Delta\log(\Sigma M_{*,1.5R_e})$< 0.3 dex) and the difference of sSFR between each AGN and its comparison galaxies to be within 0.3 dex ($\Delta\log(\mathrm{sSFR}_{1.5R_e})$ <0.3). These two constraints ensure the AGN and comparison galaxies to have the same levels of disc star formation as characterized by the SFRs and sSFRs. With the MaNGA-produced H α maps, we can make consistent measurements of the disc SFRs for all objects. In addition, by fixing the star formation level at 1.5 Re, we can assure any difference in the inner region is due to the central activity instead of the global offset. These qualities are measured by data products in MaNGA MPL_6.

Here, we did not control the global SFRs because: (i) The SFR measurements using MaNGA data only are also not consistent because the coverage of IFU bundle to different galaxies varies (Bundy et al. 2015; Wake et al. 2017). (ii) The total SFR is not consistently measured for the MaNGA galaxies. The SFR derived by Salim et al.

(2016) and Chang et al. (2015) are not well compatible with each other at lower sSFRs. (iii) The inner SFR/sSFR that also contributes to the total SFR of galaxy is the quality we want to compare between the AGN and comparison galaxies.

(6) The difference in central stellar mass surface density between each AGN and its comparison galaxies to be within $\Delta\Sigma M_{*,0.3R_e} < 0.5$ dex: this quantity could further constrain the central structure (Fang et al. 2013), and avoid the effect of any spatially resolved SFR/stellar-mass relationship on the central star formation.

2.5 The measurements of spatially resolved sSFRs

With the selection of AGNs with star-forming discs and comparison star-forming galaxies, we then carried out measurements of the spatial-resolved specific star formation rate (sSFR). Here, the specific star formation rate refers to the star formation rate divided by the stellar mass, which qualifies the current stellar mass growth rate. We used the attenuation corrected H α flux map to estimate the spatial-resolved SFR (Kennicutt 1998). The stellar mass surface density of MaNGA galaxies are measured using PIPE3D (Sánchez et al. 2016a,b). A Salpeter initial mass function is assumed. Attenuation correction applied to Hα flux assumed the case B Balmer decrement (H α/H β = 2.87) and the extinction law of Calzetti (2001).

For the central part of the AGNs where the emission comes from both SMBH accretion and star formation, we tried to estimate the SFRs through decomposition. The contribution from star formation in the Balmer emission line could be derived if the intrinsic [O III]/H β line ratio of AGN emission is known. The observed [O III] 5007Å and H β emission line flux in the central region of these 14 type 2 AGNs could be contributed by both star formation and AGN narrow line region, thus the [O III]/H β ratio could be expressed as equation (1)

$$\frac{F^{\rm obs}_{\rm [OIII]5007}}{F^{\rm obs}_{\rm H\beta}} = \frac{F^{\rm AGN}_{\rm [OIII]5007} + F^{\rm SF}_{\rm [OIII]5007}}{F^{\rm AGN}_{\rm H\beta} + F^{\rm SF}_{\rm H\beta}}. \quad (1)$$

The right part of the equation (1) could also be written in forms of [O III]/H β line ratios of star formation and AGN narrow line region.

$$\frac{F^{\rm obs}_{\rm [OIII]5007}}{F^{\rm obs}_{\rm H\beta}} = \frac{F^{\rm AGN}_{\rm [OIII]5007}}{F^{\rm AGN}_{\rm H\beta}} \times \frac{F^{\rm AGN}_{\rm H\beta}}{F^{\rm obs}_{\rm H\beta}} + \frac{F^{\rm SF}_{\rm [OIII]5007}}{F^{\rm SF}_{\rm H\beta}} \times \frac{F^{\rm SF}_{\rm H\beta}}{F^{\rm obs}_{\rm H\beta}}. \quad (2)$$

The superscripts tell the origin of the emission lines (AGNs, star-forming region or the observed total emission line flux). The total emission line flux and their line ratio are observables that could be derived directly from MaNGA data while the line ratio at AGN NLR and need to be determined with other information (see the following paragraph and Section 4.1 for the discussion). Then the contribution of star formation in Balmer emission line could be derived based on the observed [O III]/H β line ratio using the equation (3) with assumptions on the [O III]/H β line ratio of AGNs and star formation base spectra. From equation (3), we could express the $\frac{F^{\rm SF}_{\rm H\beta}}{F^{\rm obs}_{\rm H\beta}}$ at the end of equation (2) as:

$$\frac{F^{\rm SF}_{\rm H\beta}}{F^{\rm obs}_{\rm H\beta}} = \frac{(F^{\rm AGN}_{\rm [OIII]5007}/F^{\rm AGN}_{\rm H\beta}) - (F^{\rm obs}_{\rm [OIII]5007}/F^{\rm obs}_{\rm H\beta})}{(F^{\rm AGN}_{\rm [OIII]5007}/F^{\rm AGN}_{\rm H\beta}) - (F^{\rm SF}_{\rm [OIII]5007}/F^{\rm SF}_{\rm H\beta})}. \quad (3)$$

The [O III]/H β value for pure star formation in equation (3) are determined for each galaxy individually, as it is sensitive to the metallicity (Maiolino et al. 2008). We measured the average of [O III]/H β in different radial bins with a width of 0.1Re, among which the lowest value is used as the ([O III]/H β) of pure star formation. For the pure AGN line ratio, we applied log([O III]/H β) = 1.0 with a error of ±0.2. This brackets two cases: the value of log([O III]/H β) = 0.8 has previously been used in a similar analysis by Kauffmann & Heckman (2009), and a value of log([O III]/H β) = 1.2 is similar to the value of the upper bound of all SDSS AGNs and also the maximum of our selected AGNs. The uncertainties of log([O III]/H β) value in AGN region is the major source of error in the estimation central SFR($\sim$ 0.2–0.3dex), while the high S/N of MaNGA spectra makes contribution of measurement error of emission line flux to be minimal in this process.

3 RESULTS

3.1 Properties of AGNs and their host galaxies

The general properties of 14 AGNs and their host galaxies are listed in Table 1. We derived the [O III] luminosity from the reduced MaNGA datacube. The lower and upper limit of $L_{\rm [O\,III]}$ are calculated from the integrated [O III] flux within central 2 arcmin and that of all regions classified as composite or AGN/LINER in BPT diagram. We collected the total SFR and total stellar mass of each galaxy from large multiwavelength value-added catalogues of (Chang et al. 2015; Salim et al. 2016). Our AGNs samples have luminosities that are typical of Seyfert galaxies and most of their host galaxies have late type morphology and high stellar masses ($\log(M/{\rm M}_\odot > 10.5)$). We also cross-matched our sample with the FIRST Survey Catalogue (Helfand, White & Becker 2015) to obtain their properties in radio emission. 7 out of 14 AGNs in our sample have FIRST detection with S/N>5. Three of them have 1.4 GHz luminosity higher than the prediction of their total SFRs by more than 0.5 dex using converting factor from Kennicutt & Evans (2012), which probably suggests the existence of radio jet or outflows (Ho 2008; Zakamska et al. 2016; Hwang et al. 2018).

3.2 Star formation in AGN host galaxies

To compare the spatially resolved sSFRs between AGNs and normal galaxies, we plotted the SFR surface density versus stellar mass surface density (Σ_*) of all spaxels within five radial bins ($< 0.3\ R_e$, 0.3–0.6 R_e, 0.6–0.9 R_e, 0.9–1.2 R_e, and 1.2–1.5 R_e) for each AGN and its comparison sample, respectively. Both quantities are corrected for the galaxy inclinations derived from the photometric axis ratio in NASA_Sloan Atlas[1] (Blanton et al. 2011). The linear fitting to the relation between $\log(\Sigma_{\rm SFR})$ and $\log(\Sigma_{\rm M_*})$ in each radial bin was then performed for AGNs and comparison galaxies, respectively. With the slope fixed to a unity, the interceptions of the linear fitting give the sSFR in each radial bins. The log(sSFR) as a function of the galactocentric radii for each AGN and their comparison galaxies are shown in the final panel of each row in the Figs 3 and 4. The relation between Σ_{M_*} and $\Sigma_{\rm SFR}$ is actually sub-linear as previous studies suggested (Sánchez et al. 2013; Cano-Díaz et al. 2016) However, the selection of the slope does not significantly affect the measured sSFR in each radial bins. We could derive similar sSFRs as the fitting method even when calculating the mean sSFR in each radial bins. The central sSFRs of LINERs are used as upper limits given that they could have intrinsically lower [O III]/H β values than Seyferts, which causes an overestimate of their central SFRs in our analysis.

[1] http://nsatlas.org

Table 1. SFR and 1.4 GHz luminosity 14 MaNGA AGNs.

MaNGA Plate-IFU	z	Log($L_{[O\ III]}$)[a]	Log($L_{1.4\ GHz}$)[a]	Log(SFR$_{1.4GHz}$)[b]	Log(SFR$_{SED}$)[b]	Log(SFR$_{22micron}$)[b]	Log($M/M_\odot$)[c]
8147–6102	0.063 1	41.07 ± 0.14	<29.04	<0.837	0.712 ± 0.142	0.454	11.06
8241–6102	0.037 3	41.54 ± 0.11	29.56	1.362 ± 0.006	0.407 ± 0.053	1.291	10.63
8317–12704	0.054 3	41.09 ± 0.12	<28.90	<0.697	−0.011 ± 0.230	N/A	11.36
8459–3702[d, e]	0.072 2	41.01 ± 0.15	29.57	1.370 ± 0.025	0.660 ± 0.192	0.548	11.25
8588–12704	0.030 4	41.05 ± 0.13	28.43	0.235 ± 0.056	−0.111 ± 0.287	N/A	10.90
8606–12701	0.063 3	41.29 ± 0.13	<29.04	<0.839	0.479 ± 0.024	0.367	11.39
8718–12701	0.049 9	41.13 ± 0.12	<28.81	<0.619	0.436 ± 0.247	0.262	10.86
8718–12702[d]	0.038 9	41.00 ± 0.11	29.08	0.881 ± 0.018	0.146 ± 0.138	0.377	10.71
9047–6104[d]	0.058 6	41.46 ± 0.11	29.81	1.610 ± 0.009	0.534 ± 0.164	1.052	11.27
9095–12701	0.087 5	41.22 ± 0.10	<29.34	<1.144	0.498 ± 0.244	0.739	11.31
9182–12703	0.068 8	41.24 ± 0.11	<29.12	<0.916	0.247 ± 0.133	0.608	11.21
9196–12703	0.081 9	42.00 ± 0.13	29.59	1.386 ± 0.031	0.919 ± 0.118	1.201	11.37
9485–12705	0.032 3	41.35 ± 0.12	<28.42	<0.222	0.221 ± 0.081	1.236[f]	11.05
9508–12704	0.080 9	41.37 ± 0.09	29.66	1.455 ± 0.024	$0.192^{+0.385}_{-3.615}$	N/A	11.37

Notes. [a] In ergs s^{-1}. [b] In $M_\odot$ yr^{-1}. [c] In $M_\odot$. [d] Radio luminosity exceeds the prediction of star formation.
[e] Blob source in (Wylezalek et al. 2017). [f] Identified as MIR AGN, SFR_{SED} likely overestimated.
References: (1) This Work; (2) Salim et al. (2016); (3) Chang et al. (2015); (4) Helfand et al. (2015).

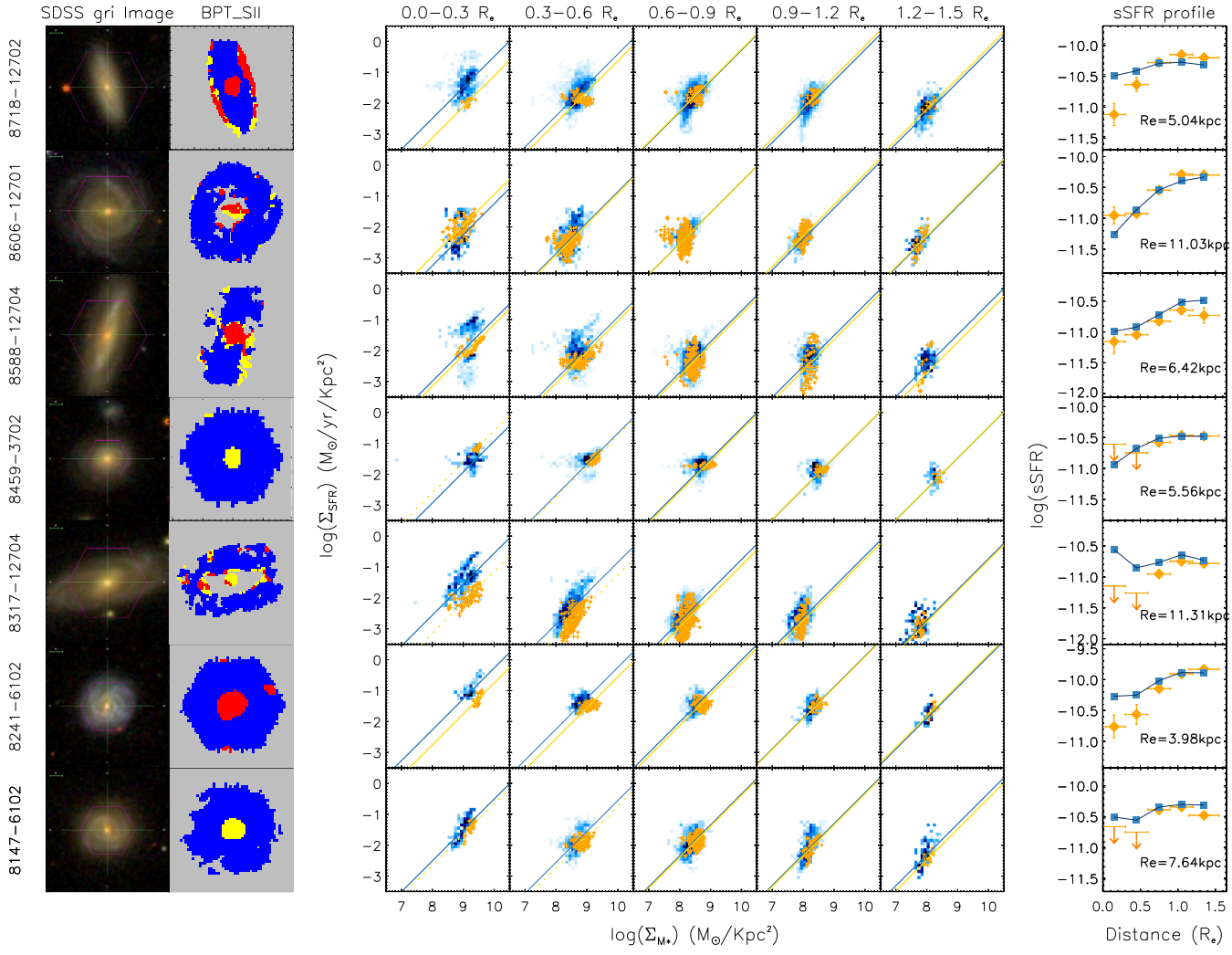

Figure 3. Our selected AGN sample and their star-forming properties in five radial bins. From left to right: the *gri* false-colour images of AGN host galaxies with MaNGA IFU footprint overlaid; the BPT maps of AGN host galaxies based on the emission line flux maps produced by PIPE3D; the SFR surface density versus stellar mass surface density in five radial bins for AGNs (yellow points) and their control normal galaxies (blue points), where the lines are the best linear fitting to AGNs (brown) and normal galaxies (pink), respectively; dashed lines are fitting of bins dominate by non-star-forming emission in AGN host galaxies; the mean sSFRs (interceptions of the best linear fits) of AGNs and normal galaxies as a function of radii.

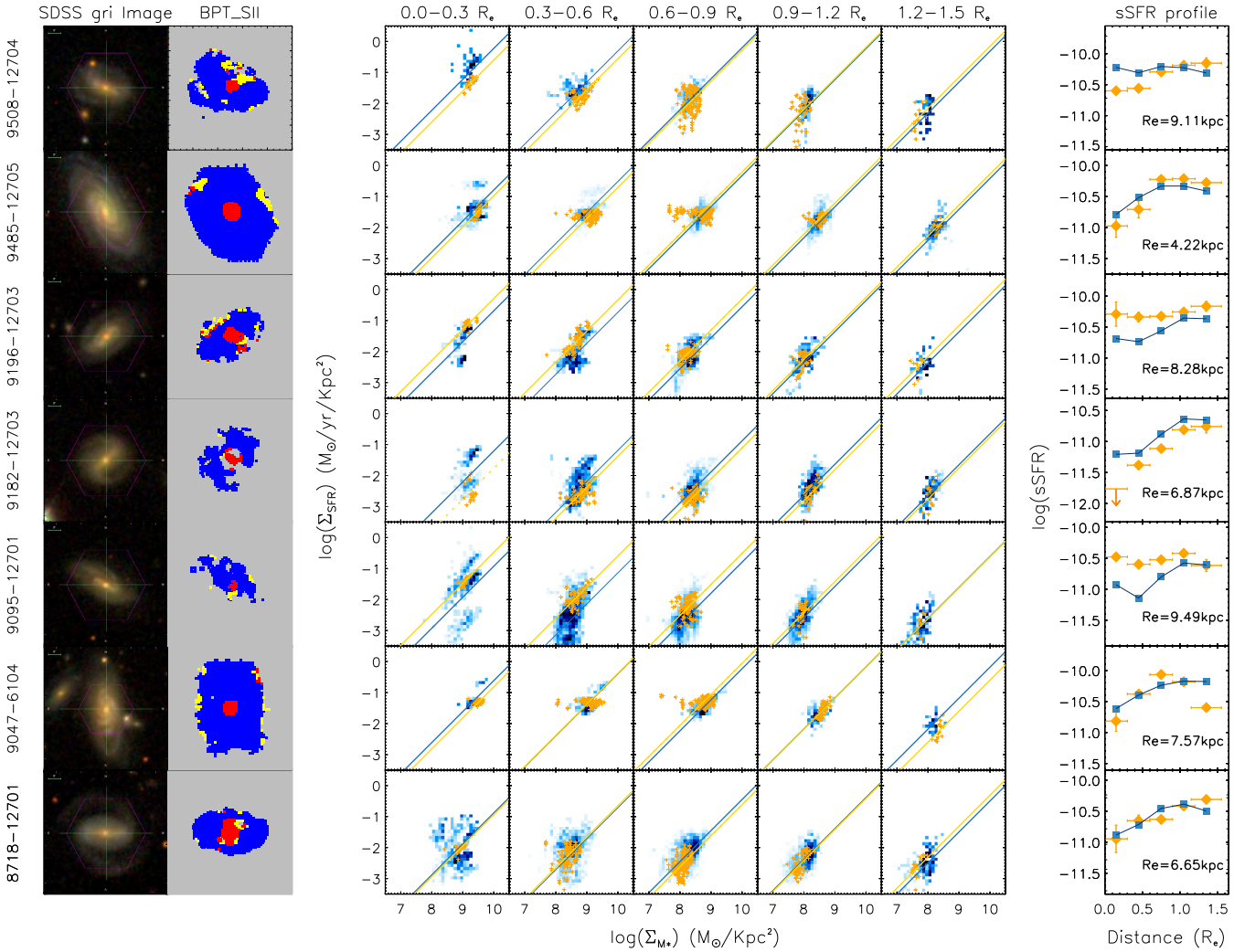

Figure 4. The same as Fig. 3 but for additional seven objects.

The distributions of the differences in the sSFRs (Δlog(sSFR)) between AGNs and their comparison normal galaxies are shown as filled histograms in Fig. 5 for each radial bin. In the inner two bins ($<0.3R_e$ and 0.3–0.6R_e), the offsets in sSFRs are systematically biased towards negative values, implying possible negative feedback. In outer radial bins (0.6–0.9, 0.9–1.2, and 1.2–1.5 R_e), Δlog(sSFR) has a median value around zero, indicating that the star formation of AGNs are not different from pure star-forming galaxies. As listed in Table 2, 10 out of 14 AGNs have Δlog(sSFR) < 0.0 in the central bin, with 5 AGNs below -0.25 and 3 AGNs below -0.5.

To compute the statistical significance of these offsets, we drew a group of star-forming galaxy with matched physical properties of AGNs and measured their Δlog(sSFR). We used the AGN comparison sample of 75 star-forming galaxies and for each of them we selected a control sample using the same methods as we did for the AGN sample. Then we measured Δlog(sSFR) of each star-forming galaxy from its comparison star formation galaxies. The star symbols in Fig. 5 show the results. We fitted the distributions of comparison sample with Gaussian functions and derive the statistical probability as following: first to randomly draw 14 objects from the Gaussian distribution and then to compute the probability that more objects than the observed number of AGNs have Δlog(sSFR) $<$ 0.5, Δlog(sSFR) < 0.25, Δlog(sSFR) < 0.0, Δlog(sSFR) < -0.25 and Δlog(sSFR) < -0.5, e.g. for the central bin this require all 14 randomly selected galaxies with Δlog(sSFR) $< 0.5 >$ 10 galaxies with Δlog(sSFR) $< 0.0 >$ 10 AGN with Δlog(sSFR) $< 0.0 >$ 5 AGNs with Δlog(sSFR) < -0.25 and > 3 AGNs with Δlog(sSFR) < 0.5. As listed in Table 3, the probability to produce the observed Δlog(sSFR) distribution of the MaNGA Seyferts from star formation galaxies ($P(N_{AGN}) < P(N_{SF})$) is as low as 0.76 per cent in the innermost bin and 3.5 per cent in the second radial bin, supporting that the central regions of AGNs most likely have suppressed SFRs.

4 DISCUSSION

4.1 The emission line flux decomposition

Some assumptions are made about the decomposition of the central emission line fluxes. We consider the observed fluxes of central emission lines are the superposition of the emission from massive young stars and that from SMBH accretion. Under such assumption, a similar method has been applied to high spatial resolution IFU spectra of some nearby galaxies (Davies et al. 2014, 2016). They decomposed the emission line by using the intrinsic spectra of different ionization mechanisms (star formation, AGNs or shock). However, the poor spatial resolution of MaNGA data (about factor

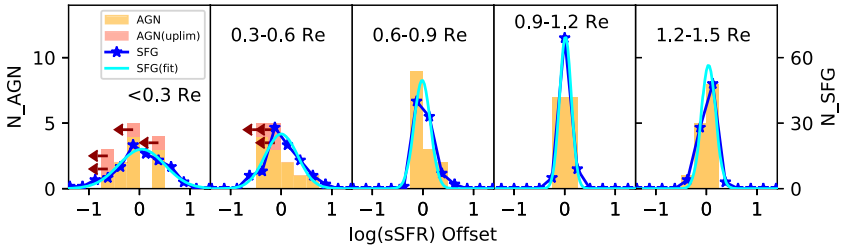

Figure 5. The distribution of the difference in the log(sSFR) between AGNs and their comparison normal galaxies. The histograms are for our AGNs, the symbols are the 'fake AGN' that are randomly retrieved from normal galaxies with matched properties of AGN host galaxies. The solid line is the best fitted Gaussian profile to the fake AGNs. From left to right, the distributions are shown for five radial bins.

Table 2. Numbers of AGNs with suppressed star formation in two central radial bins.

Radial bin	$\Delta\log(\mathrm{sSFR}) < -0.00$	$\Delta\log(\mathrm{sSFR}) < -0.25$	$\Delta\log(\mathrm{sSFR}) < -0.50$
0.0-0.3 R_e	10/14	5/14	3/14
0.3-0.6 R_e	10/14	5/14	0/14

Table 3. The probability to draw the $\Delta\log(\mathrm{sSFR})$ distribution of MaNGA Seyferts from star formation galaxies with similar or even lower value.

Radial bin	$P(N_{\mathrm{AGN}}) < P(N_{\mathrm{Control}})$
0.0–0.3 R_e	0.76%
0.3–0.6 R_e	3.5%

of 5 larger in the real physical scale per spaxel) causes significant blending between the emission from star-formation regions and AGN NLR regions, making it hard to find an central spaxel with purely star formation region or AGN NLR emission. This dilution could be supported by the much lower maximum [O III]/H β line ratio in some MaNGA AGNs compared to that in high spatial resolution IFU data (Davies et al. 2016) and to the largest values of all SDSS samples (e.g. Brinchmann et al. 2004). To overcome caveats due to our low spatial resolutions, we adopted fixed maximal line ratios of AGNs, which, if any, causes the derived SFRs to be overestimated, thus strengthening our conclusions of suppresses central SFRs in AGN hosts.

Our decomposition method also assumes the same Balmer decrement for AGN NLRs narrow as star-forming H II regions. Previous studies of local AGNs have found that AGN NLRs do have similar dust extinctions to the H II regions in their host galaxies (Wild et al. 2011; Trump et al. 2015), which holds over a large range of obscuration. Since our AGN samples are also selected optically, it is unlikely that they have different internal dust extinction properties compared to AGNs in Wild et al. (2011) and Trump et al. (2015). Significantly larger extinction in single H II region has been seen in the ENLR of Centaurs A from high-resolution observations (Salomé et al. 2016). However, the derived young age makes this H II region an extreme among extragalactic H II regions. And the poor spatial resolution of the MaNGA fibre makes the observation only sensitive to kpc-scale average extinction, which is similar to studies of Wild et al. (2011) and Trump et al. (2015). If we consider the higher intrinsic Balmer decrement in AGN-dominated regions (Osterbrock & Ferland 2006), the central star formation rate corrected by the case B value could be slightly overestimated, while this does not dramatically change the main results.

We examined the reliability of our SFR measurements of our AGNs through the relation between central SFR and black hole accretion rate (BHAR) as found in Diamond-Stanic & Rieke (2012).

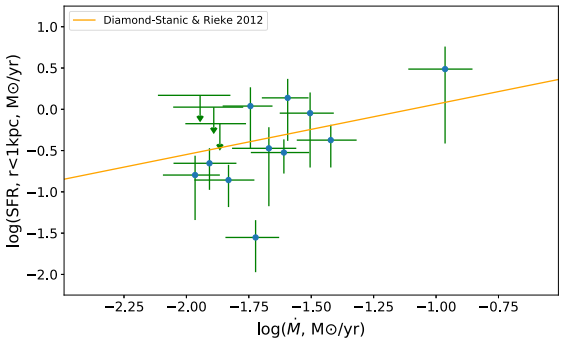

Figure 6. The distribution of our AGNs on the plot of the nuclear SFR versus BHAR where the solid line is the best-fitting one in the literature (Diamond-Stanic & Rieke 2012).

They derived the SFRs using the mid-infrared aromatic features that are insensitive to the dust extinction and contamination by AGNs. We used our decomposition method to derive the SFR within the same aperture (<1kpc) as in Diamond-Stanic & Rieke (2012) and the BHAR from the [O II] luminosity (Kauffmann & Heckman 2009) for all our 14 AGNs. As shown in Fig. 6, our derived SFRs and BHARs in general follows the relation as found by Diamond-Stanic & Rieke (2012), suggesting the reliability of our SFR measurements.

4.2 Implications of AGN feedback on star formation

Based on the data of 14 AGNs, our analysis shows a marginal suppression of star formation within central few kpc. This result suggests moderate luminosity AGNs could regulate the star formation in host galaxies. AGN outflows in ionized gas are detected in some of our samples by the residual flux at high velocity (in the range of blueshifted by 500–1000 km s^{-1}) after subtracting the Gaussian-fitted narrow emission line and stellar continuum from the spectra. Fig. 7 shows the distribution of outflow signals with S/N>3 per pixel for six of our sample. Most of these detected outflow are confined to the central few arc-seconds where suppressed star formation is identified. The small-scale outflows could probably be more pervading in the sample than we identified, since the spatial resolution and low radial velocity of outflowing gas limit the

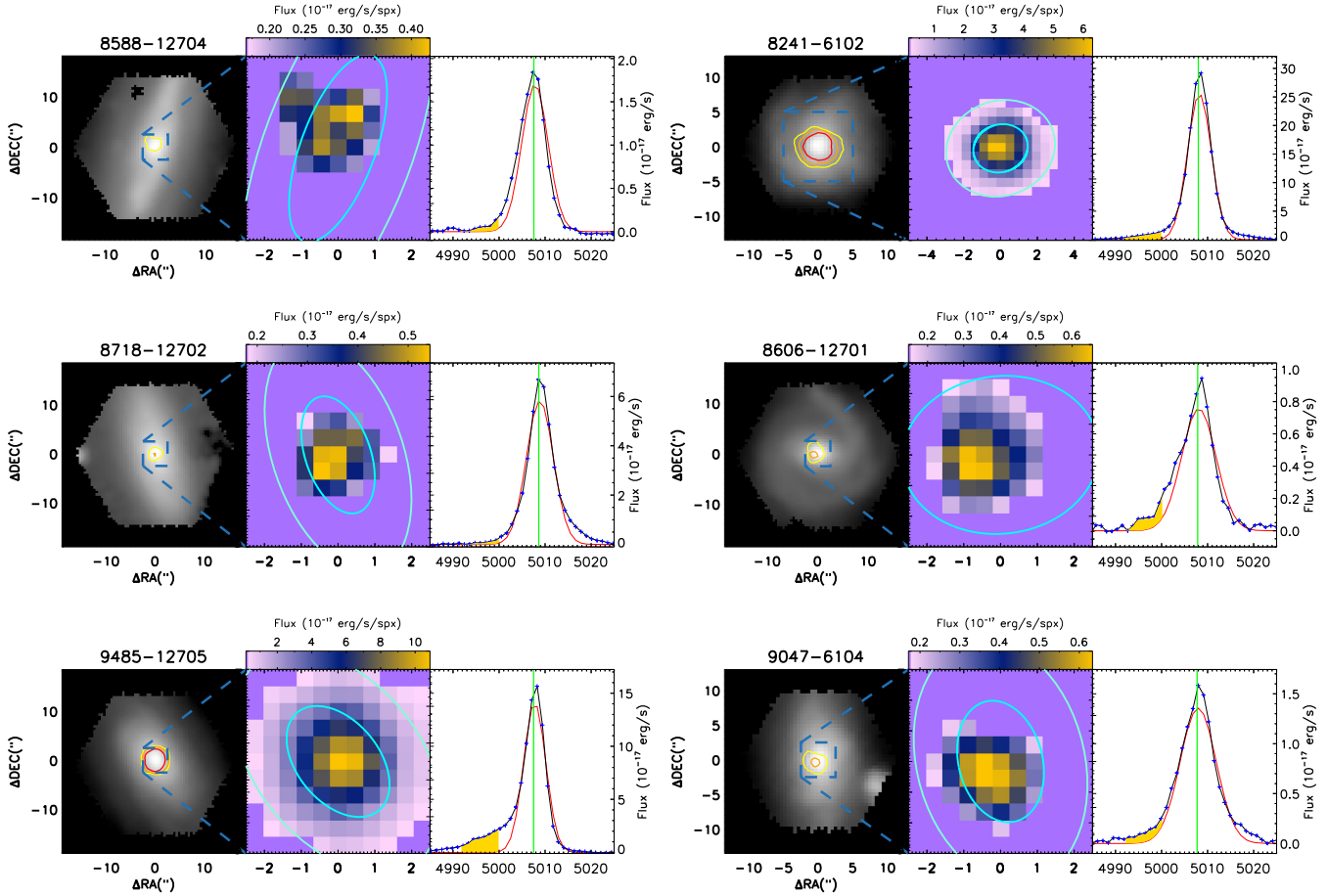

Figure 7. The 6 AGNs with [O III]5007Å outflows. For each object, from left to right, the broad-band image with the distribution of outflow S/N overlaid, where the yellow, orange, and red con tour correspond to S/N equals to 3, 7.5, and 25, respectively; the map of [O III]5007Å outflow strength (integrated between -500 and $-1000\,\mathrm{km\,s^{-1}}$); the integrated [O III]5007Å line from the central 1 arcsec where the filled yellow region indicates the outflow. The inner and outer ellipse represents the projected circle with radius of $0.25R_e$ and $0.5R_e$.

detection rate under this coarse method (see Wylezalek et al. (2017) for an example, 8459–3702, which is also included in our sample).

It is possible that the outflows co-spatial with the low-SFR region cause the star formation suppression. However, in some cases the ability of ionized gas outflows to impact the central star formation is questioned, as they could only carry limited energy and momentum that is not likely to significantly influence the dense gas and the star formation therein (Balmaverde et al. 2016; Bae et al. 2017). In recent studies, more convincing evidence of AGN feedback on star formation has been revealed by the discovery of growing number of AGNs with outflows that could remove dense molecular gas within the central region of the host galaxies (Cicone et al. 2014; García-Burillo et al. 2014), which is more closely related to ongoing star formation in galaxies. However, single dish observations still find similar central molecular gas mass and gas fraction in local AGNs as compared normal galaxies whose stellar mass and morphology are controlled to be the same (Rosario et al. 2018), indicating that the outflow can not significantly impact the dense molecular gas content of the galaxies. This is consistent with our finding that central SFRs in AGNs are only mildly suppressed.

Besides the feedback by outflow, moderate to low-luminosity AGNs could also impact the star formation by the kinetic energy carried in small-scale jets (Guillard et al. 2015; Querejeta et al. 2016), which represent another probable paradigm of AGN feedback in Seyfert galaxies. Enhancement in turbulence caused by the interaction between outflows/jets with ambient gas could provide additional support against the self gravity, suppressing the collapse of gas clouds and star formation. For our samples, we find not all of our AGNs detected in radio continuum show lower sSFR in their centres. This might be caused by the small physical scale of regions affected by jets compare to MaNGA's resolution. The gas distribution in general follow rotational disc of host galaxies, while the orientation of jets are not strongly correlated with the large-scale angular momentum of galaxies. As a result the jets could interact with the dense molecular gas and probably impact the star formation in their host galaxies only when the jets are nearly coplanar with the discs and dense ISM is distributed along their path.

In our study, we measured the star formation rate by H α emission (Kennicutt & Evans 2012) that trace short-lived (10 Myrs) O stars. Our optical selection of AGNs also only sensitive to SMBHs undergo active accretion of gas, which generally has a duration of 10^7–10^8 yr (Haehnelt & Rees 1993; Novak, Ostriker & Ciotti 2011). Therefore, our result reflects the impact of current AGN activity on the recent star formation in host galaxies. Literatures usually refers to this kind of feedback coherent with AGN activity as fast mode of feedback (Alexander & Hickox 2012; Cresci & Maiolino 2018; Harrison et al. 2018), where the radiation/outflow/jet released dur-

ing the accretion of SMBHs directly impact the star formation. Fast mode feedback has been suggested to be responsible for the fast star formation quenching in major mergers triggering luminous quasars (Springel 2005; Hopkins et al. 2006), which probably result in the massive non-active galaxies at higher redshift. Our results suggest that it probably also have mild impact on the star formation in local disc galaxies.

A growing number of studies supported a generally long quenching time-scale in local quiescent galaxies (Schawinski et al. 2014; Peng, Maiolino & Cochrane 2015; Belfiore et al. 2017; Sánchez et al. 2018). These studies pointed out that it is the gradual exhaustion of internal gas or (and) the secular growth of central bulges that contributes most to the galaxy quenching in local Universe, which acts at time-scales of around 1 Gyrs. Studies on the integrated colours of late type galaxies indicated that AGNs in these galaxies are in favour of more aged stellar population than galaxies that have just started quenching, which does not support a casual link between global quenching of late type galaxies and nuclear activities (Schawinski et al. 2010, 2014). However, it might be difficult for previous studies to search for spatially limited AGN feedback on star formation using integrated physical qualities of galaxies. Our discovery of marginally suppressed star formation within central kpc of MaNGA AGNs provide evidence that the fast removal/exhaustion of gas by AGN feedback could also act as an important process in the quenching of central part of secular evolved galaxies, in addition to the slower quenching process that has been widely suggested.

Alternative explanations to our finding such as the AGNs in favour of more aged stellar populations exceeding the lifetime of massive hot stars could also be plausible, which has been suggested by previous study like Norman & Scoville (1988) and Davies et al. (2007). They suggest the slower stellar wind from aged stars could provide material more easily accreted by central black holes accretion. Recent studies have also revealed qualitatively similar overabundance of stellar population within the central 0.5 Re of some more luminous MaNGA AGNs (Rembold et al. 2017; Mallmann et al. 2018). However, comparing to our studies, these works either focus on stellar population at much smaller physical scales, or use a different controlling method in their comparison. In order to reveal if these results and our finding reflect different sides of interaction between AGNs and central star formation in host galaxies, more detailed studies on the stellar population of current sample are needed.

5 CONCLUSION

We investigated the spatially resolved star formation in 14 local Seyfert galaxies with the IFU observations by the SDSS-IV MaNGA survey. For each of 14 AGNs, we carefully selected a set of normal galaxies with the total stellar mass, bulge-to-disc ratio, central stellar mass surface density and specific star formation rate at 1.0–1.5R_e controlled to be the same. We derive the specific star formation rates of 14 Seyfert galaxies within five radial bins measured from IFU spectra and compared with those of the control sample. The comparison shows that the central radial bins of AGNs have slightly lower SFRs with false-positive possibilities of 0.76 per cent in the innermost 0.3 Re and 3.5 per cent within the 0.3–0.6 Re. These low possibilities indicate marginally suppressed star formation within the central region of our AGNs. This may suggest that moderate SMBH accretion is capable of regulating star formation at the galaxy centres.

ACKNOWLEDGEMENTS

The authors thank Yifei Jin, Christy Tremonti, and Renbin Yan for their valuable suggestions. LB and YS acknowledge support from the National Key R&D Program of China (No. 2018YFA0404502), the National Natural Science Foundation of China (NSFC grants 11733002 and 11773013), the Excellent Youth Foundation of the Jiangsu Scientific Committee (BK20150014), and National Key R&D Program of China (No. 2017YFA0402704). YC acknowledge support from the National Natural Science Foundation of China (NSFC grants 11573013). SFS thank the Consejo Nacional de Ciencia y Tecnología (CONACyT) program CB-180125 and Dirección General Asuntos del Personal - Programa de Apoyo a Proyectos de Investigación e Innovación Tecnológica (DGAPA-PAPIIT) IA101217 grants for their support to this project. RM acknowledges support by the Science and Technology Facilities Council (STFC) and from the ERC Advanced Grant 695671 'QUENCH'. RR thanks to Conselho Nacional de Desenvolvimento Científico e Tecnológico (CNPq) and Fundação de Amparo À Pesquisa do Estado do Rio Grande do Sul (FAPERGS). DB is supported by grant Russian Science Foundation (RScF) 14-50-00043.

Funding for the Sloan Digital Sky Survey IV has been provided by the Alfred P. Sloan Foundation, the U.S. Department of Energy Office of Science, and the Participating Institutions. SDSS-IV acknowledges support and resources from the Center for High-Performance Computing at the University of Utah. The SDSS web site is www.sdss.org.

SDSS-IV is managed by the Astrophysical Research Consortium for the Participating Institutions of the SDSS Collaboration including the Brazilian Participation Group, the Carnegie Institution for Science, Carnegie Mellon University, the Chilean Participation Group, the French Participation Group, Harvard-Smithsonian Center for Astrophysics, Instituto de Astrofísica de Canarias, The Johns Hopkins University, Kavli Institute for the Physics and Mathematics of the Universe (IPMU) / University of Tokyo, Lawrence Berkeley National Laboratory, Leibniz Institut für Astrophysik Potsdam (AIP), Max-Planck-Institut für Astronomie (MPIA Heidelberg), Max-Planck-Institut für Astrophysik (MPA Garching), Max-Planck-Institut für Extraterrestrische Physik (MPE), National Astronomical Observatories of China, New Mexico State University, New York University, University of Notre Dame, Observatário Nacional / MCTI, The Ohio State University, Pennsylvania State University, Shanghai Astronomical Observatory, United Kingdom Participation Group, Universidad Nacional Autónoma de México, University of Arizona, University of Colorado Boulder, University of Oxford, University of Portsmouth, University of Utah, University of Virginia, University of Washington, University of Wisconsin, Vanderbilt University, and Yale University.

This project makes use of the MaNGA-Pipe3D dataproducts. We thank the IA-UNAM MaNGA team for creating this catalogue, and the ConaCyt-180125 project for supporting them.

This research made use of Marvin, a core PYTHON package and web framework for MaNGA data, developed by Brian Cherinka, José Sánchez-Gallego, and Brett Andrews (MaNGA Collaboration 2017).

REFERENCES

Alam S. et al., 2015, ApJS, 219, 12
Alatalo K. et al., 2015, ApJ, 798, 31
Alexander D. M., Hickox R. C., 2012, New Astron. Rev., 56, 93

Bae H.-J., Woo J.-H., Karouzos M., Gallo E., Flohic H., Shen Y., Yoon S.-J., 2017, ApJ, 837, 91
Baldwin J. A., Phillips M. M., Terlevich R., 1981, PASP, 93, 5
Balmaverde B. et al., 2016, A&A, 585, A148
Baum S. A. et al., 2010, ApJ, 710, 289
Belfiore F. et al., 2016, MNRAS, 461, 3111
Belfiore F. et al., 2017, MNRAS, 466, 2570
Blanton M. R., Kazin E., Muna D., Weaver B. A., Price-Whelan A., 2011, AJ, 142, 31
Blanton M. R. et al., 2017, AJ, 154, 28
Brinchmann J., Charlot S., White S. D. M., Tremonti C., Kauffmann G., Heckman T., Brinkmann J., 2004, MNRAS, 351, 1151
Bundy K. et al., 2015, ApJ, 798, 7
Calzetti D., 2001, PASP, 113, 1449
Cano-Díaz M., Maiolino R., Marconi A., Netzer H., Shemmer O., Cresci G., 2012, A&A, 537, L8
Cano-Díaz M. et al., 2016, ApJ, 821, L26
Carniani S. et al., 2016, A&A, 591, A28
Chang Y.-Y., van der Wel A., da Cunha E., Rix H.-W., 2015, ApJS, 219, 8
Cheung E. et al., 2016, Nature, 533, 504
Choi E., Ostriker J. P., Naab T., Oser L., Moster B. P., 2015, MNRAS, 449, 4105
Christensen L., Jahnke K., Wisotzki L., Sánchez S. F., Exter K., Roth M. M., 2006, A&A, 452, 869
Cicone C. et al., 2014, A&A, 562, A21
Cid Fernandes R., Stasińska G., Schlickmann M. S., Mateus A., Vale Asari N., Schoenell W., Sodré L., 2010, MNRAS, 403, 1036
Cresci G., Maiolino R., 2018, Nature Astron., 2, 179
Cresci G. et al., 2015, ApJ, 799, 82
Davies R. I., Müller Sánchez F., Genzel R., Tacconi L. J., Hicks E. K. S., Friedrich S., Sternberg A., 2007, ApJ, 671, 1388
Davies R. L., Kewley L. J., Ho I.-T., Dopita M. A., 2014, MNRAS, 444, 3961
Davies R. L. et al., 2016, MNRAS, 462, 1616
Diamond-Stanic A. M., Rieke G. H., 2012, ApJ, 746, 168
Drory N. et al., 2015, AJ, 149, 77
Dumas G., Mundell C. G., Emsellem E., Nagar N. M., 2007, MNRAS, 379, 1249
Fabian A. C., 2012, ARA&A, 50, 455
Fang J. J., Faber S. M., Koo D. C., Dekel A., 2013, ApJ, 776, 63
Feruglio C. et al., 2015, A&A, 583, A99
Forman W. et al., 2007, ApJ, 665, 1057
García-Burillo S. et al., 2014, A&A, 567, A125
Guillard P., Boulanger F., Lehnert M. D., Pineau des Forêts G., Combes F., Falgarone E., Bernard-Salas J., 2015, A&A, 574, A32
Gunn J. E. et al., 2006, AJ, 131, 2332
Haehnelt M. G., Rees M. J., 1993, MNRAS, 263, 168
Harrison C. M., 2017, Nature Astronomy, 1, 0165
Harrison C. M. et al., 2012, MNRAS, 426, 1073
Harrison C. M., Alexander D. M., Mullaney J. R., Swinbank A. M., 2014, MNRAS, 441, 3306
Harrison C. M., Costa T., Tadhunter C. N., Flütsch A., Kakkad D., Perna M., Vietri G., 2018, Nature Astron., 2, 198
Heckman T. M., Best P. N., 2014, ARA&A, 52, 589
Helfand D. J., White R. L., Becker R. H., 2015, ApJ, 801, 26
Ho I.-T. et al., 2014, MNRAS, 444, 3894
Hopkins P. F., Hernquist L., Cox T. J., Di Matteo T., Robertson B., Springel V., 2006, ApJS, 163, 1
Hopkins P. F., Torrey P., Faucher-Giguère C.-A., Quataert E., Murray N., 2016, MNRAS, 458, 816
Ho L. C., 2008, ARA&A, 46, 475
Hwang H.-C., Zakamska N. L., Alexandroff R. M., Hamann F., Greene J. E., Perrotta S., Richards G. T., 2018, MNRAS, 477, 830
Karouzos M. et al., 2014, ApJ, 784, 137
Kauffmann G., Heckman T. M., 2009, MNRAS, 397, 135
Kauffmann G. et al., 2003, MNRAS, 346, 1055
Kennicutt R. C., Jr., 1998, ARA&A, 36, 189
Kennicutt R. C., Jr., Tamblyn P., Congdon C. E., 1994, ApJ, 435, 22
Kennicutt R. C., Evans N. J., 2012, ARA&A, 50, 531
Kewley L. J., Dopita M. A., Sutherland R. S., Heisler C. A., Trevena J., 2001, ApJ, 556, 121
Kewley L. J., Groves B., Kauffmann G., Heckman T., 2006, MNRAS, 372, 961
King A., 2003, ApJ, 596, L27
Kormendy J., Ho L. C., 2013, ARA&A, 51, 511
Krause M., Fendt C., Neininger N., 2007, A&A, 467, 1037
Law D. R. et al., 2015, AJ, 150, 19
Law D. R. et al., 2016, AJ, 152, 83
López-Cobá C. et al., 2017a, MNRAS, 467, 4951
López-Cobá C. et al., 2017b, ApJ, 850, L17
Maiolino R. et al., 2008, A&A, 488, 463
Maiolino R. et al., 2012, MNRAS, 425, L66
Mallmann N. D. et al., 2018, MNRAS, 478, 5491
Morganti R., Oosterloo T., Oonk J. B. R., Frieswijk W., Tadhunter C., 2015, A&A, 580, A1
Norman C., Scoville N., 1988, ApJ, 332, 124
Novak G. S., Ostriker J. P., Ciotti L., 2011, ApJ, 737, 26
Osterbrock D. E., Ferland G. J., Osterbrock D. E., Ferland G. J., 2006, Astrophysics of Gaseous Nebulae and Active Galactic Nuclei. Univ. Science Books, Sausalito, CA
Peng Y., Maiolino R., Cochrane R., 2015, Nature, 521, 192
Querejeta M. et al., 2016, A&A, 593, A118
Rembold S. B. et al., 2017, MNRAS, 472, 4382
Riffel R., Riffel R. A., Ferrari F., Storchi-Bergmann T., 2011, MNRAS, 416, 493
Riffel R. A., Storchi-Bergmann T., Riffel R., Dahmer-Hahn L. G., Diniz M. R., Schönell A. J., Dametto N. Z., 2017, MNRAS, 470, 992
Roos O., Juneau S., Bournaud F., Gabor J. M., 2015, ApJ, 800, 19
Rosario D. J. et al., 2018, MNRAS, 473, 5658
Salim S. et al., 2016, ApJS, 227, 2
Salomé Q., Salomé P., Combes F., Hamer S., Heywood I., 2016, A&A, 586, A45
Sánchez S. F. et al., 2013, A&A, 554, A58
Sánchez S. F. et al., 2014, A&A, 563, A49
Sánchez S. F. et al., 2016a, Rev. Mex. Astron. Astrofis., 52, 21
Sánchez S. F. et al., 2016b, Rev. Mex. Astron. Astrofis., 52, 171
Sánchez S. F. et al., 2018, Rev. Mex. Astron. Astrofis., 54, 217
Schawinski K. et al., 2010, ApJ, 711, 284
Schawinski K. et al., 2014, MNRAS, 440, 889
Shi Y. et al., 2007, ApJ, 669, 841
Shi Y., Rieke G. H., Ogle P., Jiang L., Diamond-Stanic A. M., 2009, ApJ, 703, 1107
Shi Y., Helou G., Yan L., Armus L., Wu Y., Papovich C., Stierwalt S., 2011, ApJ, 733, 87
Shi Y., Armus L., Helou G., Stierwalt S., Gao Y., Wang J., Zhang Z.-Y., Gu Q., 2014, Nature, 514, 335
Shi Y. et al., 2018, ApJ, 853, 149
Silk J., 2013, ApJ, 772, 112
Simard L., Mendel J. T., Patton D. R., Ellison S. L., McConnachie A. W., 2011, ApJS, 196, 11
Smee S. A. et al., 2013, AJ, 146, 32
Springel V., 2005, MNRAS, 364, 1105
Stasińska G. et al., 2008, MNRAS, 391, L29
Trump J. R. et al., 2015, ApJ, 811, 26
Wake D. A. et al., 2017, AJ, 154, 86
Wang J., Fabbiano G., Karovska M., Elvis M., Risaliti G., 2012, ApJ, 756, 180
Wild V. et al., 2011, MNRAS, 410, 1593
Wild V. et al., 2014, A&A, 567, A132
Willett K. W. et al., 2013, MNRAS, 435, 2835
Wylezalek D., Zakamska N. L., 2016, MNRAS, 461, 3724
Wylezalek D. et al., 2017, MNRAS, 467, 2612
Xu L., Rieke G. H., Egami E., Haines C. P., Pereira M. J., Smith G. P., 2015, ApJ, 808, 159
Yan R., Blanton M. R., 2012, ApJ, 747, 61
Yan R. et al., 2016a, AJ, 151, 8

Yan R. et al., 2016b, AJ, 152, 197
Zakamska N. L. et al., 2016, MNRAS, 455, 4191
Zhang Z., Shi Y., Rieke G. H., Xia X., Wang Y., Sun B., Wan L., 2016, ApJ, 819, L27
Zinn P.-C., Middelberg E., Norris R. P., Dettmar R.-J., 2013, ApJ, 774, 66
Zubovas K., Bourne M. A., 2017, MNRAS, 468, 4956
Zubovas K., Nayakshin S., King A., Wilkinson M., 2013, MNRAS, 433, 3079

This paper has been typeset from a TEX/LATEX file prepared by the author.